Analytical and Bioanalytical Chemistry
https://doi.org/10.1007/s00216-022-04309-8

PAPER IN FOREFRONT

An ultrasensitive and disposable electrochemical aptasensor for prostate-specific antigen (PSA) detection in real serum samples

Canan Özyurt[1] · İnci Uludağ[2] · Mustafa Kemal Sezgintürk[2]

Received: 27 June 2022 / Revised: 22 August 2022 / Accepted: 29 August 2022

Abstract

In this study, we constructed a disposable indium tin oxide polyethylene terephthalate film (ITO-PET)-based electrochemical aptasensor for analyzing prostate-specific antigen (PSA), one of the most important biomarkers of prostate cancer. Because of their clinical importance, building PSA biosensing systems with high sensitivity and stability is essential. However, it still presents significant difficulties, such as low detection limits. We designed a platform to covalently bind the amino-terminated aptamer by modifying the ITO-PET surface with carboxyethylsilanetriol (CTES) to obtain a self-assembled monolayer (SAM). We also evaluated the potential for use in real human serum samples by investigating the optimal operating conditions and analytical performance characteristics of the developed biosensor. The design we present here exhibits excellent precision, with a limit of detection (LOD) as low as 8.74 fg/mL PSA. The broad linear detection range of the biosensor under optimal conditions was determined as 1.0–1500 fg/mL. The dissociation constant (K_d) for the aptamer was also calculated as 46.28 ± 5.63 nM by evaluating the impedimetric response as a function of PSA concentration. The aptasensor displayed considerable repeatability (1.3% RSD) and reproducibility (7.51% RSD) and good storage stability (98.34% of the initial activity for 8 weeks). Additionally, we demonstrated that the technique we developed was quite efficient in estimating the kinetics of aptamer–analyte interactions by determining the K_d and single-frequency impedance (SFI) data. In conclusion, we proposed a selective and sensitive biosensor with the potential for clinical application and superior performance in real serum samples.

Keywords Aptamer · Aptasensor · Prostate-specific antigen · Biosensor · Prostate cancer · Electrochemical impedance spectroscopy

Introduction

Prostate cancer (PC) is among the most commonly diagnosed cancer in men. About 3.8% of PC cases diagnosed in 2020 resulted in death [1]. Survival rates are significantly improved when PC is detected in its early stages [2]. In efforts to find alternatives to biopsy-based methods, which are painful and can lead to relatively late diagnosis, studies have been carried out for years using many different noninvasive biomarkers for early PC diagnosis. One of the most commonly used biomarkers in PC diagnosis is prostate-specific antigen (PSA). PSA is a serine protease produced in abundance in both normal and cancerous prostate epithelium. PSA is released into the bloodstream in trace amounts by a healthy prostate. However, PSA levels are increased considerably in individuals with prostatic disease, and serum PSA levels above 4 ng/mL are generally considered abnormal [3].

The PSA test is only one tool used to screen for early signs of PC. The clinical behavior of PC may be asymptomatic, and its symptoms are often not present at the time of diagnosis. In most cases, an elevated PSA level raises clinical suspicion of PC. A digital rectal exam (DRE) is another screening test, usually performed following a PSA test. While these may be signs of PC, they require additional evaluation. If there are adjustable variables that may

Published in the topical collection *Electrochemical Biosensors – Driving Personalized Medicine* with guest editors Susana Campuzano Ruiz and Maria Jesus Lobo-Castañón.

✉ Mustafa Kemal Sezgintürk
msezginturk@comu.edu.tr

[1] Department of Chemistry and Chemical Processing Technologies, Lapseki Vocational School, Çanakkale Onsekiz Mart University, Çanakkale, Turkey

[2] Bioengineering Department, Engineering Faculty, Çanakkale Onsekiz Mart University, Çanakkale, Turkey

Published online: 26 September 2022

temporarily increase PSA levels, these factors should be addressed before repeating the PSA test. Additionally, urological evaluation is useful for establishing whether a prostate biopsy is required, whether further testing may reduce the need for biopsy at that time, and when a reassessment should occur [4]. A clinical determination is made as to whether a biopsy is necessary based on the PSA test, DRE, and other ancillary test findings. During a prostate biopsy, tissue samples from the prostate are taken for further analysis. The results of the biopsy are used to establish a diagnosis of cancer. A negative prostate biopsy result may not exclude the potential for PC. Even in PC cases, a prostate biopsy can miss malignant cells owing to the sampling method, even when imaging is employed to guide the biopsy. Possible side effects of biopsy include serious infections, pain, and bleeding. In PSA screening, false-positive test findings are also prevalent. Consequently, a second biopsy may be necessary if the PSA level rises [5]. In non-biopsy-based clinical studies, antibody-based autoanalyzer systems are frequently used. However, today's relatively traditional methods also have some limitations regarding measuring serum PSA levels, especially low detection limits. The literature notes that both internationally agreed threshold levels and high PSA level values have a large margin of error [6]. Moreover, the study of antibody cross-reactions in antibody-based autoanalyzer systems used in hospitals is crucial, including chemiluminescence-based methods [7]. Since only the main reference materials (World Health Organization [WHO] reference materials) have been established, and PSA lacks a complete reference measurement system comprising reference materials and reference measurement techniques, the standardization of PSA tests used in clinical laboratories is limited [8]. The importance of developing proof-of-concept detection systems is better understood by considering the need for standardized methods in the clinic.

In contrast to biopsy-based approaches, which cause possible side effects and may result in relatively late diagnosis, several possible indicators, including PSA, for early detection of PC have been studied by researchers. Pro-PSA refers to a variety of inactive forms of PSA. In addition, PSA appears in the blood in multiple structural isoforms (IsoPSA). The IsoPSA test analyzes the total spectrum of PSA isoforms and can be used to identify men at high risk of developing PC where biopsy is needed [9]. Traditional PSA determination methods and their updated versions are still used for the analysis of serum PSA levels, including enzyme-linked immunosorbent assay (ELISA) [10, 11], chemiluminescence immunoassay (CLIA) [12, 13], electrochemiluminescence immunoassay (ECLIA) [14], radioimmunoassay (RIA) [15], and fluorescence-based assays [16]. Some of the conventional methods have also been adapted to clinical usage. Although these procedures are effective and highly precise, they are time-consuming, costly, and labor-intensive.

Among the studies on PSA detection, biosensor-based approaches are promising for early diagnosis, providing highly sensitive measurements. Compared with the time-consuming and costly procedures often employed in healthcare, biosensors provide a better alternative because of their sensitivity, selectivity, ease of use, and ability to be deployed in situ. Researchers have created hundreds of unique biosensing systems for PSA detection over the past few decades. Sensitive PSA determination has been achieved in studies with various methodologies including electrochemical methods [17, 18], optical detection systems [19, 20], and mass-based platforms [21, 22].

Early PSA biosensors mostly used antibody-based approaches, but other recognition components, including nucleic acid sequences, polymers, and aptamers, are gaining popularity today [23]. Aptamers are single-stranded DNA (ssDNA) or ssRNA oligonucleotides that can identify many targets with great sensitivity and specificity. Over the past few years, nucleic acid aptamers have become more popular in diagnostics and biosensor development. Aptamers are a more effective alternative to antibodies in many aspects. They are less costly, have higher chemical stability, and are simpler to generate than antibodies. In contrast to antibodies, the in vitro selection process may be adjusted to the required pH, temperature, and ionic strength. Aptamers can also be straightforwardly manipulated, and their architectures are compatible with many media and matrices. Thanks to the benefits of aptamers, high-precision PSA biosensors have been designed by different research groups [17, 24].

Aptamers are also frequently used in different electrochemical methods, including electrochemical impedance spectroscopy (EIS). The EIS technique uses sinusoidal electric potential to study electrode surface changes. EIS measures electrode resistance and capacitance to detect biological interactions, quantifying aptamer–antigen interactions as electrical impulses without labeling or pretreatment. Biosensors based on EIS have advantages over other electroanalytical methods, such as direct recognition without labeling the relationships between recognition elements and analytes, a nondestructive nature, and steady-state system. These features are also useful for defining analytical parameters related to the binding kinetics and interfacial properties and for analyte detection [25–27].

In this study, we developed an EIS-based PSA aptasensor using ITO-PET as working electrodes. To our knowledge, the PSA-specific aptamer sequence we utilized as the recognition element in this study represents the first such use on a carboxyethylsilanetriol (CTES)-modified surface on ITO-PET electrodes. ITO-PET electrodes are transparent conductive oxide films. Their use in biosensor design offers several advantages over traditional electrode systems,

including excellent electrical conductivity, low cost, and an extensive working surface. Within the scope of this study, PSA detection with femtomolar sensitivity was performed using the aptasensor, the analytical parameters of the relevant biosensor were defined in detail, and the potential for use in real samples for PSA analysis was evaluated. With adequate accuracy and reproducibility, the electrochemical PSA aptasensor offers a promising platform for clinical applications.

Material and methods

Chemicals and equipment

All compounds used were of analytical purity. Unless otherwise specified, all compounds were obtained from Sigma-Aldrich (USA). Bovine serum albumin (BSA) was purchased from Sigma Aldrich (USA). Electrochemical studies were conducted with a Gamry Reference 600 potentiostat/galvanostat (Gamry Instruments, Warminster, PA, USA). Ferri/ferro redox probe solution was prepared by mixing 5 mM $[Fe(CN)_6]^{4-}$ and 5 mM $[Fe(CN)_6]^{3-}$ in phosphate buffer (PB; pH 7) containing 0.1 M KCl. ITO film covered on polyethylene terephthalate (PET) film with a surface resistivity of 60 Ω/sq (639303-1EA) was purchased from Sigma-Aldrich (USA). ITO-PET electrodes (2 mm x 20 mm) were used in a three-electrode arrangement, along with an Ag/AgCl reference electrode and a platinum wire counter electrode. The solutions were prepared using the Elga PURELAB flex pure water equipment, weighed with a Shimadzu Corporation ATX224 instrument, and measured using a Fisher Scientific pH meter. Scanning electron microscopy (SEM, JEOL SEM-7100) and atomic force microscopy (AFM, WITec alpha3100R) were used to determine the surface morphology. The 5′-NH_2-$(CH_2)_6$-TTTTTAATTAAAGCTCGCCATCAAATAT-3′ PSA aptamer sequence was provided by Macrogen. Serum samples were taken from Namık Kemal University Research Hospital, with the approval of the ethics committee.

Electrochemical analyses

All electrodes used in immobilization procedures were treated with PSA solutions of varying concentrations. EIS and cyclic voltammetry (CV) experiments describe the surface behavior at various PSA concentrations and each optimization step. Electrochemical measurements were taken inside the redox probe. The applied voltage for CV measurements was set between 0.5 V and 1 V, with a step size of 10 mV and a sweep rate of 100 mV/s. The standard measurement potential for impedance is 0 V and 5 mV for alternating current. Impedance was measured between 50,000 and 0.001 Hz.

Construction of a biosensing system for PSA analysis

The ITO-PET electrodes were cleaned by ultrasonication in acetone, soap solution, and ultrapure water for 10 min each, followed by dehydration at room temperature using argon gas. The electrodes were then submerged for 90 min in a 5:1:1 (v/v) solution of ultrapure water, hydrogen peroxide, and ammonium hydroxide to create hydroxylated active ITO-PET surfaces under dark conditions. They were then rinsed with ultrapure water and dried with argon gas. The hydroxylated ITO-PET electrodes were placed in a 0.1–0.5% CTES (v/v) solution prepared with ultrapure water at room temperature overnight. The CTES-modified ITO-PET electrodes were washed with ultrapure water and dried with argon gas. Before aptamer immobilization, electrode surfaces were treated using carbodiimide (EDC)/*N*-hydroxysuccinimide (NHS) chemistry. EDC (0.04 M) as a coupling agent and NHS (0.01 M) as an activator were used to activate the CTES-modified ITO-PET electrodes. After rinsing the ITO-PET electrodes with ultrapure water to remove any unbound EDC/NHS, the electrodes were placed in a PB solution (pH 7.0) with a PSA aptamer. Before each use, the aptamer was folded into the correct conformation by incubation at 95 °C for 10 min, 10 min on ice, and 10 min at 25 °C, after which 0.1 µM PSA aptamer was immobilized on the modified electrode for 30 min. The amino groups (NH_2) of the PSA aptamer formed a strong amide bond (CO–NH) with the carboxyl groups of the modified ITO-PET electrodes. Subsequently, aptamer-modified electrode surfaces were blocked with 0.5% BSA. After this final step, the electrodes were fully functional for PSA measurement. During trials to determine the best settings, different concentrations of PSA ranging from 1 to 1500 fg/mL were added to the modified electrodes. As seen in Fig. 1, each change in the ITO-PET electrode was confirmed by EIS and CV, and charge-transfer resistance (R_{ct}) values were obtained for each concentration using EIS measurements ($n = 3$). These values were calculated using the following equation:

$$\Delta R_{ct} = Rct_{(PSA)} - Rct_{(BSA)}$$

Optimization studies for PSA Analysis

To analyze the effects of CTES concentration on the hydroxylated ITO-PET electrode surface, different concentrations of CTES (0.1, 0.25 and 0.5%) were applied while maintaining fixed concentrations of other immobilization components. The EIS and CV data with

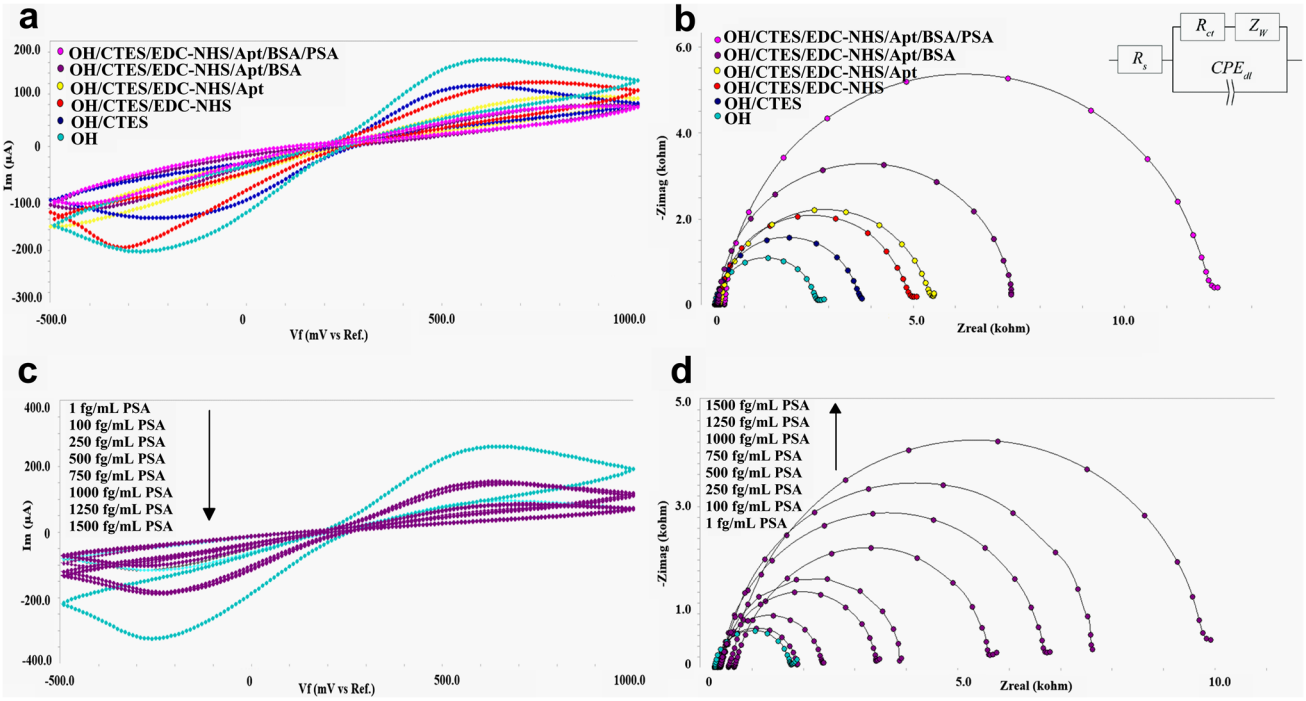

Fig. 1 **a** Voltammetric and **b** impedimetric characterization of the buildup process of the immunosensor (the concentration values and composition of the components used in the immobilization stage are as follows: CTES: 0.1%; H_2O_2-NH_4OH-H_2O: 1:1:5 (v/v); EDC/NHS: 0.04–0.01 M; PSA aptamer: 0.1 µM; BSA: 0.5% and PSA: 1500 fg/mL). **c** CV and **d** EIS responses of the immunosensor at elevated PSA concentrations (1, 150, 250, 500, 750, 1000, 1250, 1500 fg/mL PSA), respectively

increasing PSA concentrations for the independently prepared electrodes were examined, and the graphs in the linear range were compared. To determine the effect of aptamer concentration to be supplied to the optimized CTES-modified ITO-PET electrode, EIS and CV measurements were performed against different concentrations of PSA aptamer (0.1, 0.25 and 0.5 µM) for 30 min. After optimization of the PSA aptamer incubation time, the incubation time of PSA-antigen on the modified ITO-PET electrode was optimized for 30, 45, and 60 min. To achieve this optimization, EIS and CV measurements were conducted on the aptamer-modified ITO-PET electrode that was incubated at varied periods and PSA concentrations. Optimization parameters were used to construct the calibration plot for the PSA aptamer-based PSA biosensor.

Characterization studies for PSA analysis

The reproducibility of the biosensor was tested with the modified ITO-PET electrodes fabricated at different times and under ideal conditions. For this investigation, 10 different biosensor systems were developed, and EIS measurements were made within the detection range of the proposed biosensor. For the repeatability analysis, 20 distinct ITO-PET electrodes were fabricated. The mean value, standard deviation value, and coefficient of variation were determined using EIS measurements of these electrodes, incubated at the chosen concentration. Furthermore, the interaction between the PSA aptamer and PSA antigen was assessed by observing how the impedance changed over time at a single frequency. Impedimetric measurements were taken at the selected PSA concentration (750 fg/mL) of different electrodes prepared under the same conditions and stored for 10 weeks to determine the storage life of the designed biosensor system (in a dark, dry environment at +4 °C). SEM and AFM techniques were also used in each immobilization phase to observe the immobilization processes on the electrode surface.

Calculations for the determination of the analytical parameters

To determine the analytical parameters, the difference in the electron transfer resistance ($R_{ct(PSA)}$) value at a certain concentration of PSA from the electron transfer resistance ($R_{ct(BSA)}$) value of the BSA application, which is the last immobilization step, was used. The following equation was used to construct the calibration graph and the binding plot for the PSA aptasensor:

$$\Delta R_{ct} = R_{ct(PSA)} - R_{ct(BSA)}$$

In this equation, $R_{ct(PSA)}$ and $R_{ct(BSA)}$ are the semicircular diameter values recorded after the PSA application and BSA blocking stage, respectively, while ΔR_{ct} indicates the difference between these two values. The limit of detection (LOD) and limit of quantitation (LOQ) are the minimum measured and quantified concentrations. The equations 3 σ/m and 10 σ/m were subsequently used to determine LOD and LOQ [28, 29]. In these equations, σ is the standard deviation of the blank signal, and m represents the slope of the calibration curve.

K_d was calculated by applying PSA at concentration values above the dynamic range and evaluating the graph with the nonlinear regression (specific binding with the hill slope) function of GraphPad Prism 5.0 software [30]. To determine the K_d value, the ΔR_{ct} responses were plotted against PSA concentrations [31]. The following equation was used for the calculation, in which the ΔR_{ct} values obtained by taking the $R_{ct(PSA)} - R_{ct(BSA)}$ difference were plotted against the PSA concentration using the Hill equation [32]:

$$\Delta R_{ct} = \frac{B_{max} \cdot [PSA]^h}{K_d{}^h + [PSA]^h}$$

K_d represents the concentration of ligand that binds to half of the equilibrium receptor sites. B_{max}, K_d, and h are the interpolated PSA concentrations at which the maximum biosensor response is reached, the PSA concentration required to achieve the half-maximum biosensing signal, and the Hill coefficient, respectively.

Selectivity of the PSA biosensor

In order to evaluate the selectivity of the developed immunosensor, several components (glucose, ascorbic acid, BSA, haptoglobin, and immunoglobulin G [IgG]) were utilized during the detection of the PSA antigen. Concentrations of interfering components were created with the PB at 500 fg/mL, and EIS and CV measurements were carried out under optimal circumstances ($n = 3$).

Evaluation of the applicability of the biosensor to serum samples

After immobilization and characterization investigations, real serum samples (serum samples were taken from Namık Kemal University Research Hospital with approval by the ethics committee) were used to test the designed biosensor system. According to recent studies, a PSA level of 4.0 ng/mL is appropriate [33]. According to this value, serum samples were diluted 10,000-fold with PB and tested using the standard analyte addition procedure. Following this step, human serum samples were spiked with PSA standards (250 and 500 fg/ml). The immunosensor was used to examine the prepared solution, and the findings are given in Table 1.

Results and discussion

Fabrication of the aptasensor

Scheme 1 depicts the fabrication of the label-free ITO-PET aptasensor. In the first two successive stages of the design of the aptasensor, following the formation of hydroxyl groups on the ITO-PET electrode, the electrode surface was functionalized by the CTES silanization process [34]. CTES is a carboxyl group-containing silane coupling agent, and EDC/NHS treatment activates these carboxyl groups. As a result of the amide bond formed by the active carboxyl groups of the developed SAM with the 5′-amino-modified PSA aptamer, the relevant aptamer sequences were immobilized on the electrode surface. In the final step in constructing a fully functional detector electrode, BSA (0.5%) was applied to block the possible active sites that may be present on the electrode surface. The prepared ITO-PET/CTES/EDC-NHS/PSA aptamer/BSA electrodes were washed with ultrapure water and dried with argon gas before use in studies to investigate the high-sensitivity detection of PSA.

Table 1 Suitability of the PSA biosensor for use with real serum samples

Serum sample number	PSA conc. (fg mL^{-1})	Standard added conc. (fg mL^{-1})	Measured conc. (fg mL^{-1}, $n = 3$)	RSD (%) ($n = 3$)	Recovery (%)
1	208.77	250	486.16/478.29/466.35	3.95	103.95
		500	719.84/696.82/722.76	0.61	100.61
2	532.19	250	749.56/735.29/791.81	2.98	97.02
		500	1112.03/942.16/1061.33	0.61	100.61
3	625.15	250	898.75/806.67/851.84	2.59	97.41
		500	1173.81/1016.75/1226.25	1.23	101.23
4	660.11	250	891.17/935.75/910.99	0.28	100.28
		500	1176.72/1189.83/1071.53	1.21	98.79
5	225.38	250	503.64/443.91/453.23	1.78	98.22
		500	743.74/723.63/751.31	1.95	101.95

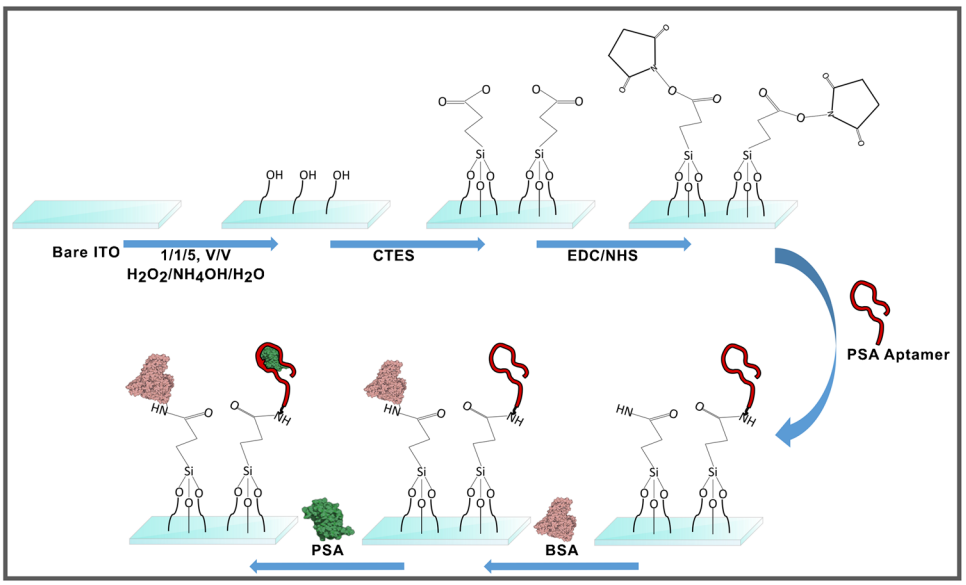

Scheme 1 Schematic illustration of the construction process of the PSA aptasensor

Determining the ideal circumstances for the construction of an effective biosensor is crucial. The establishment of parameters where appropriately oriented recognition components are suitable for generating a homogeneous layer is made possible by determining these requirements. In this regard, EIS and CV measurements confirmed the layer evolution processes on the electrode surface at each step. The EIS Nyquist plots and CV measurements of each immobilization step revealed that the insulation of the surface increased. Figure 1b (inset) depicts a Randles equivalent circuit for each EIS spectrum mentioned above. The circuit consists of the solution resistance (Rs), the R_{ct}, the Warburg resistance (Zw), and the constant phase element (CPE). The Randles equivalent circuit simulation was used to fit the impedance values, and the results corresponded to the Randles model [35]. The electron transfer resistance, R_{ct}, is depicted by the semicircle diameter in EIS, and it provides information on the electron transfer rates of the redox probe at the electrode interface. A charged layer exerts either an attractive or a repulsive force on ions close to the electrode, which can enormously impact the R_{ct} value [36, 37]. Figure 1b shows the changes in the EIS spectra after each immobilization step. It was determined that the semicircle diameter increased due to the insulation of the EDC/NHS compared with the CTES application, which was the previous immobilization stage. A striking increase in R_{ct} value was observed after covalent bonding of PSA aptamer, probably due to its nonconductive properties as well as the effects of steric hindrance and the negative charge of the phosphate group of the aptamers having electrostatic repulsion to the probe [38]. Furthermore, the amide bond formed between the amino-modified aptamer and the carboxylic acid on the surface reduces the conductivity, which is also reflected in the R_{ct} value [39]. Blocking the remaining active sites by BSA also caused an increase in the R_{ct} value due to the insulating effect of the modified ITO-PET electrode. The EIS results revealed that the proposed aptasensor was effectively configured. Immobilizing biological recognition components is crucial to creating an efficient biosensor system. Each immobilization layer must be well-organized. In the current study, CTES was applied to the ITO-PET surface to form a SAM, which was then activated by EDC/NHS chemistry. SAMs enable the development of biosensor platforms with enhanced efficiency and performance. In addition, the development of the SAM on the ITO-PET surface widened the working scale and enhanced the analytical performance. Combining these modifications has created a biosensor platform with improved performance that is more efficient and sensitive.

Investigating the electrochemical properties of modified electrodes is often done via CV. Figure 1a shows the CV results after each modification applied to the electrode surface. By evaluating the differences in oxidation and reduction peak currents in CV values associated with electrode modification steps, it was determined that each immobilization step led to an increase in the insulating properties of the ITO-PET electrode and a decrease in peak current values. The CV data provided conclusive evidence that the electrode was successfully constructed.

Surface characterization of the PSA aptasensor

SEM and AFM were used to characterize the surface morphology of the PSA aptasensor at different immobilization stages. The SEM and AFM images of a homogeneous surface with a narrow allocation on the hydroxylated ITO-PET electrode can be seen in Fig. 2a and b. The root mean square (RMS) roughness value of the ITO-PET/OH electrode was

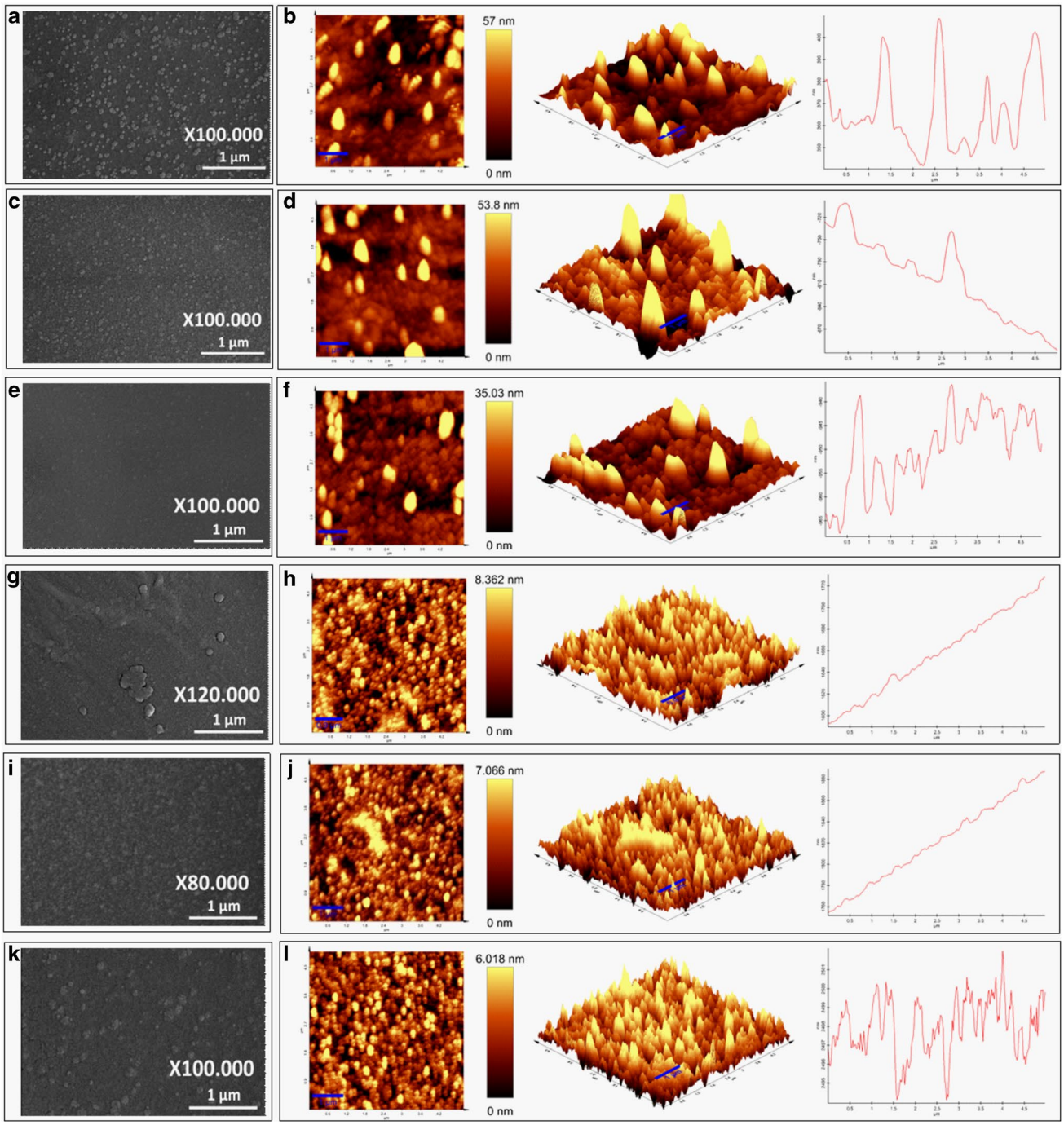

Fig. 2 SEM and AFM images of the hydroxylated ITO electrode (**a**, **b**). CTES-modified electrode surface (**c**, **d**). EDC/NHS-activated CTES-modified electrode surface (**e**, **f**). PSA aptamer-immobilized electrode surface (**g**, **h**). BSA blockage (**ı**, **j**). Surface characteristics after interaction of PSA with PSA aptamer (**k**, **l**). (The concentration values and composition of the components used in the immobilization stage are as follows: H_2O_2-NH_4OH-H_2O: 1:1:5 (v/v); CTES: 0.1%; EDC-NHS: 0.04–0.01 M; PSA aptamer: 0.1 µM; BSA: 0.5% and PSA: 1500 fg/mL, respectively)

44.868 nm on a scale of 5×5 µm. As shown in Fig. 2c and d, when the SEM and AFM images were examined after the CTES treatment, a homogeneous distribution occurred, and the roughness value was calculated as 101.163 nm on a scale of 5×5 µm. It can be deduced from the cross-sectional graph of AFM after CTES application that the gaps increased, and the silane agent interacted with the –OH groups on the electrode surface (Fig. 2d) [40]. SEM and AFM images after EDC/NHS coupling agent application for activating carboxylic acid groups are shown in Fig. 2e and f. The roughness

value obtained with AFM is 163.638 nm on a scale of 5×5 µm. SEM and AFM images obtained after applying PSA aptamer, which now displays a sharper end-appearing morphology, are indicated in Fig. 2g and h, with a roughness value of 237.967 nm at a scale of 5×5 µm. SEM and AFM images recorded after immobilization of the blocking agent BSA indicate a smooth distribution (Fig. 2i and j). A roughness value of 257.074 nm on a scale of 5×5 µm was obtained for this step. In the last stage, the electrode surface morphology was investigated after PSA application (Fig. 2k and l). The interaction of PSA and PSA aptamer creates a striking change in the surface morphology, as seen in the SEM image. After the interaction of PSA with the aptamers on the fully functionalized electrode surface, a roughness value of 277,355 nm was obtained at a scale of 5×5 µm. The data on surface morphology are consistent with EIS and CV data and support the finding that the aptasensor was successfully developed.

Determination of the optimal conditions of the aptasensor

Optimization of the experimental parameters is critical for robust electrode configuration and development of the aptasensor. In this study, after optimizing the CTES ratio, PSA aptamer concentration, and the PSA aptamer incubation time, we finally determined the ideal interaction time for the PSA aptamer and PSA. The use of CTES as a silanizing agent has many advantages, perhaps the most important of which is that monolayer production is not affected by changes in ambient humidity [41]. The optimal amount of CTES may vary depending on certain physicochemical parameters and the nature of the material used [42]. CTES was used at 0.1%, 0.25%, and 0.5% (v/v) concentrations, respectively, to determine the optimal amount, and the PSA binding efficiency of the modified electrodes was evaluated by keeping other parameters constant. As seen in Fig. S1a, the lowest slope and R^2 values were obtained using 0.5% CTES. The fact that this concentration is too high to form an efficient layer is also reflected in the linearity of the graph. Considering the R^2 values of the graphs and the consistency in the impedimetric response, 0.1% CTES was determined as the optimal concentration.

The quantity of the PSA aptamer was optimized in the next step. The PSA aptamer concentration to be applied to the CTES-modified ITO-PET electrodes was tested in the micromolar range, considering the electrode surface area (average 1 cm^2). It can be assumed that 0.5 µM aptamer concentration accumulates on the electrode surface, increasing the random coupling potentials of the aptamer sequences and, more importantly, creating a steric hindrance for analyte binding. According to the graphical parameters, the most efficient aptamer concentration was 0.1 µM, and subsequent investigations were conducted with this value (Fig. S1b).

Determining the ideal interaction time for the recognition element and the analyte in biosensors is essential for obtaining consistent and reproducible results. In order to optimize the incubation time of the PSA aptamer, another important optimization parameter, immobilization, was performed for 15, 30, and 45 min. It was determined that incubation of the PSA aptamer for 30 min elicited a higher impedimetric response and was sufficient for interaction with PSA. Although linear results were obtained below or above this time, the most significant signal decrease was detected at 30 min (Fig. S1c).

The last optimization step was to examine the ideal time for the analyte incubation process. To determine the interaction time of PSA with the aptamer, PSA was applied to the modified electrodes at 30, 45, and 60 min. The optimal PSA incubation time was determined as 30 min. The linear calibration graph obtained with different PSA incubation times is shown in Fig. S1d. Although the results obtained with 30 and 45 min of interaction were very similar, due to the slope of the graph and the time advantage it provided, 30 min of PSA incubation was used in further studies. Indeed, the single-frequency impedance (SFI) measurement result is consistent with this finding. SFI is a technique that allows for evaluation of the impedance change against time at a specified frequency. This method is particularly useful for in situ determination of analyte and recognition element interaction times [43]. As seen in Fig. 4b, the interaction of the PSA aptamer and PSA was determined in real time by SFI measurement. The SFI plot confirms that the signal stabilized for approximately 30 min, and that this time was sufficient for interaction of the PSA aptamer with the PSA. It was determined that 60 min of incubation caused a significant signal decrease. The lower responses were attributed to the long-stored analyte damaging the integration of the electrode surface and exerting physical stresses.

Analytical characterization of the aptasensor

Determination of LOD, LOQ, and K_d

EIS is an excellent approach for determining the analytical parameters of the aptasensor and is an accurate and reliable method for observing the modifications that occur in the interfacial properties of the modified electrode surfaces. Because protein deposition makes electron and mass transport of the probe challenging, increases in analyte concentrations cause significant changes in the surface insulation, as evidenced in both CV and EIS findings (Fig. 1c and d). Analytical performance criteria were defined by correlating increasing PSA concentrations with R_{ct} signals obtained in EIS measurements, so that a high-sensitivity biosensor could

be designed. The linear response of the aptasensor and the kinetics of PSA binding were determined by utilizing the equivalent circuit model (Fig. 1b inset). As mentioned earlier, the basic components of this equivalent circuit are Rs, Zw and R_{ct}. The R_{ct} value, which expresses the double-layer capacitance related to the capacitance of the complex bioactive layer, differs greatly from the deposition on the electrode surface depending on the analyte binding. Therefore, R_{ct} was chosen as a reasonable criterion to evaluate the interfacial characteristics of the designed biosensor during construction [44, 45]. The analyte deposition on the electrode surface following the interaction of PSA with the aptamer causes an increase in R_{ct} for the potassium ferri/ferrocyanide redox couple in a faradaic EIS measurement [46]. The increase in the R_{ct} is proportional to the PSA concentration.

The CV and impedance spectra of the proposed aptasensor for increasing concentrations of PSA are shown in Fig. 1c and d, respectively. As seen in Fig. 1d, the semicircle diameter of the Nyquist plot, and thus the R_{ct} values, increased with increasing concentrations of PSA. The aptasensor design achieved a large dynamic range of 1.0 fg/mL to 1500 fg/mL with a coefficient of 0.9914, as seen in Fig. 3b. Indeed, the dynamic ranges of the PSA aptasensors appear quite broad (Table S1). The range we obtained is comparable to that of other PSA biosensors in the recent literature. The calibration curve exhibited a strong linear relationship between changes in R_{ct} values and PSA concentration (Fig. 3b).

LOD and LOQ were calculated as 8.74 fg/mL (0.307 fM) and 29.13 fg/mL (1.023 fM), respectively. The detection limit obtained in this study is many times lower than that of most biosensors, including commercial PSA analyses, thanks to the high sensitivity of the aptamers combined with ITO-PET electrodes [23, 47]. In this study, we used an aptamer with a well-defined structure with a 5′-TTTTTAATTAAAGCTCGCCATCAAATAGCTTT-3′ nucleotide sequence [48]. This aptamer sequence has been utilized in many biosensing studies, as seen in Table S1. Savory and colleagues used this aptamer sequence for the first time to detect PSA in the nM range by measuring the chemiluminescence signal. The EIS-based method we present here is an inherently sensitive approach correlated with the direct analyte deposition without labeling, so we were able to measure PSA with many times higher sensitivity and dynamic range compared to this work. PSA analyses have been conducted in many unique approaches, from techniques combining molecularly imprinted polymers or thiol-terminated sulfobetaine and amine-terminated versions of the same aptamer [49, 50]. Except for a few of the studies mentioned in Table S1, most sequences were used as thiol-modified, and all were preferentially modified at the 5′ end. The results obtained with modifications at the 5′ end support the idea that the binding site of this PSA aptamer is closer to the 3′ position. One study strengthened this claim by using a sandwich assay with the PSA aptamer–PSA antibody pair by modifying the aptamer from the 5′ position with ferrocene. The binding of the aptamer to PSA closer to the 3′ end allowed the free ferrocene-labeled end to be used in differential pulse voltammetry (DPV) measurements [51]. Because it improved analytical performance in earlier studies [52], we chose to use the aptamer as amino-modified from the 5′ end in this study. Major differences in analytical performance have been obtained across many different biosensor approaches due to different immobilization, modification, and measurement approaches with the same aptamer sequence (Table S1). To the best of our knowledge, only a few studies [53, 54] using the same aptamer for biosensing have achieved the high sensitivity level we obtained in this work, which corresponds to a low femtomolar range.

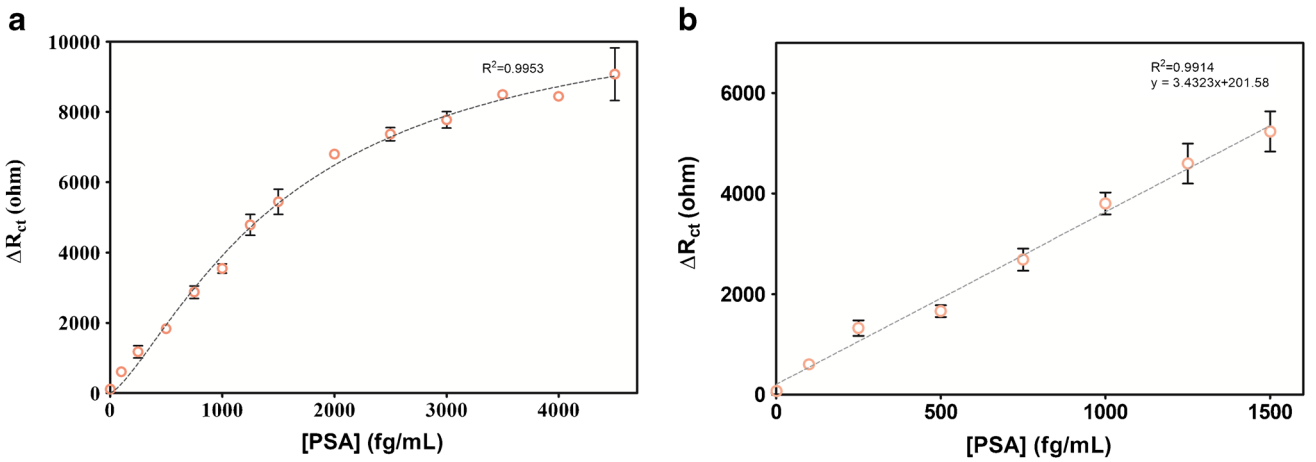

Fig. 3 **a** Binding curve for PSA, **b** calibration curve obtained after EIS measurements

K_d value calculated over impedance changes was determined as 46.28 ± 5.63 nM with a coefficient of 0.9953 for PSA aptamer by utilizing the nonlinear regression (specific binding with the hill slope) function of GraphPad Prism 5.0 software [30]. B_{max}, K_d, and h represent the interpolated PSA concentration at which the maximum biosensor response is achieved, the PSA concentration required to attain the half-maximum biosensing signal, and the Hill coefficient, respectively. The Hill coefficient describes the stoichiometry of the binding. The hill slope value was found to be 1.356 in this study. Usually, the h value greater than 1.0 is reflected on the graph sigmoidally, as shown in Fig. 3a. This value occurs when the recognition element or analyte has more than one binding site with positive cooperation [55]. Therefore, the obtained h value shows that the PSA aptamer can interact with PSA through more than one binding site. Researchers have used various methods to calculate the same aptamer's K_d. The K_d value was estimated on the nM scale in the study where the aptamer was developed for the first time [48]. Supporting the approach of the former work, in the analysis based on square wave voltammetry (SWV), fluorescence, quartz crystal microbalance (QCM), and surface plasmon resonance (SPR) for this aptamer, dissociation constants were found to be 2.6 nM, 790.27 nM, 37 nM, and 336.0 nM, respectively [56–59]. The calculated K_d value in our study is in perfect concordance with the previous data.

SFI is a method that has been successfully applied to characterize the kinetic interactions between the recognition element and the analyte in electroanalytical designs [60]. In this study, the interaction between the PSA aptamer and PSA was monitored with the SFI method, which can monitor the total impedance at a single frequency value versus time. A Bode plot was used to calculate this frequency, and the measurement was performed at a fixed frequency of 5 Hz. The impedance signal changed considerably during an interaction lasting 25–30 min, but there was no noticeable change after 30 min. This outcome demonstrates the suitability of the 30-min incubation period for interaction of the PSA aptamer and PSA (Fig. 4b).

Repeatability, reproducibility, selectivity, and storage stability studies

Repeatability is a key factor of the biosensor's long-term stability. The repeatability of the designed aptasensors was evaluated by applying 750 fg/mL PSA to the 20 identical electrodes and evaluating the obtained responses on the calibration curve. We used the calibration curve equation to compute the mean value, standard deviation, and coefficient of variation, which were 754.02 fg/mL, ±10.0, and 1.3, respectively. According to these calculations, the developed aptasensor demonstrates a high level of repeatability.

Because reproducibility is another important factor for biosensors, it was validated using 10 distinct calibration plots of biosensors that were all made under identical conditions. Within the range of 1.0 fg/mL to 1500 fg/mL, identical aptasensors exhibited a similar linearity level, as seen in Fig. 4a. The relative standard deviation was calculated from the overlapping line plots for the slopes as 7.51%. These results indicate that the reproducibility of the proposed aptasensors for the detection of PSA is satisfactory.

In addition, the Kramers–Kronig transform was used on the experimental data. In theory, Kramers–Kronig relationships may be used to evaluate whether the impedance spectrum of a given system is affected by bias errors, such as those induced by artifacts or time-dependent events [34]. Kramers–Kronig transforms were executed in this investigation using Gamry Echem Analyst software (ver. 5.61). This analysis determined a value known as goodness of fit (Fig. 4d).

In order to accurately detect their targets, biosensors need to be able to distinguish between a wide variety of analytes. Glucose, ascorbic acid, BSA, haptoglobin, and IgG were added as interfering substances to study the selectivity of the aptasensor. The analysis was also conducted with a mixture of all these potential entrepreneurs. All interfering compounds in the selectivity experiment were at 500 fg/mL final concentration. As shown in Fig. S2, most of the interfering substances had a minimal effect on the aptasensor, in contrast to the considerable increase in the R_{ct} value caused by PSA at 500 fg/mL. It was observed that glucose and ascorbic acid, relatively small molecules, interfered at very low levels. Although still far below the PSA response, the greatest interference was found to occur with BSA and IgG applications. The effect of haptoglobin, a serum protein, was less than half that of the other two proteins. It is worth noting that the same level of interference (approximately four to five times) was observed for BSA in some of the other biosensor studies designed with the same aptamer [54, 61]. Interestingly, the synergistic interference signal obtained when these components were used in the mixture was lower than the individual ones. This is probably because nonspecific binding to the aptamer becomes difficult due to the competition of molecules in the complex environment. In addition, the satisfactory results we obtained in real human serum samples indicates the advantage of our approach in the complex serum environment (Table 1). Our technique is extremely selective for PSA when the overall results are assessed.

Stability testing of biosensors is critical in evaluating how long they can be used reliably and is an essential parameter in assessing their potential in clinical applications. The biosensors prepared identically with the standard experimental immobilization procedure were stored for 10 weeks at 4 °C in dark and closed conditions. Measurements were carried out every 7 days with the prepared biosensors, and

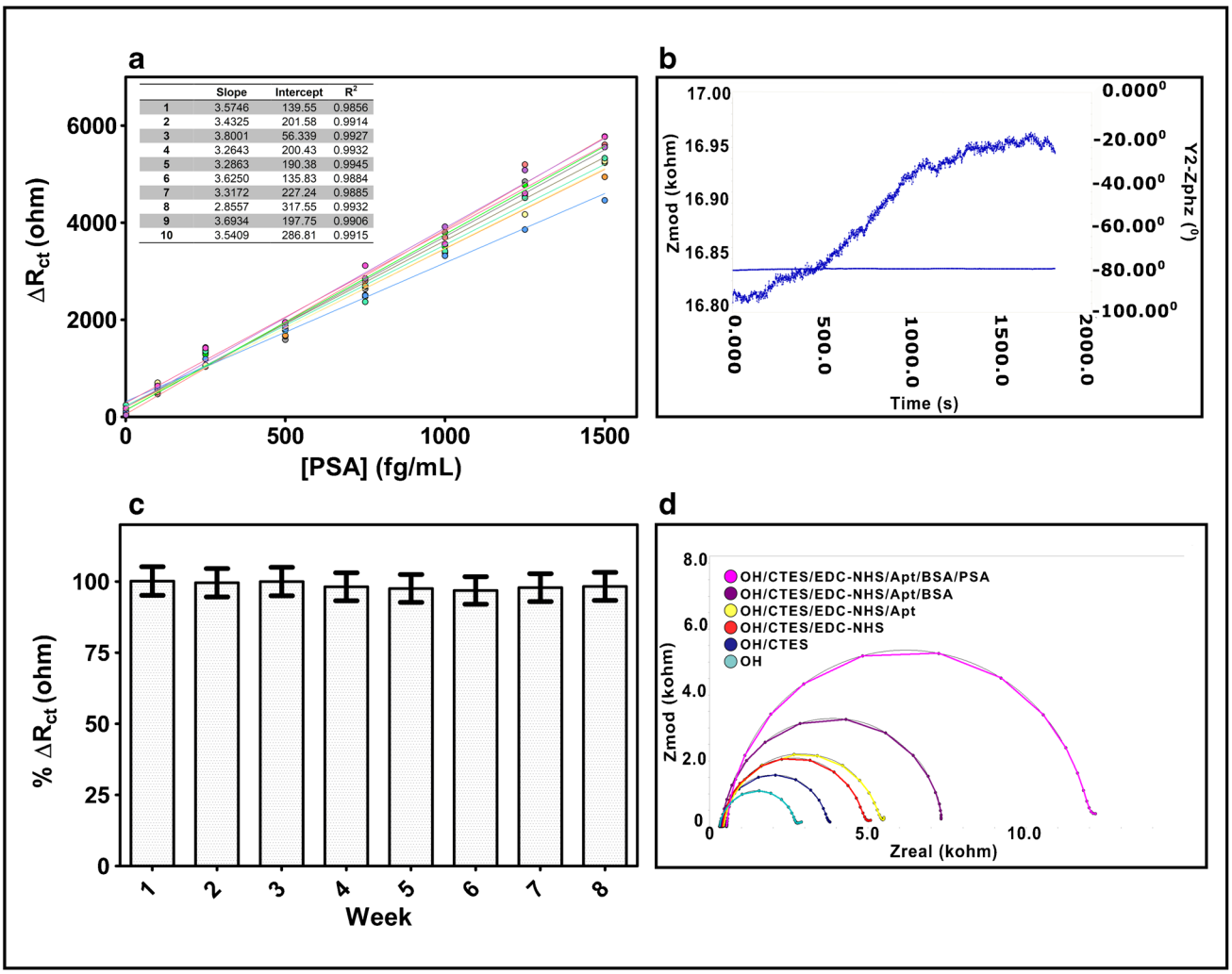

Fig. 4 **a** Reproducibility study, **b** single-frequency impedance result, **c** storage life, and **d** Kramers–Kronig transforms of the developed biosensor

the impedimetric response obtained for 750 fg/mL PSA was evaluated with the calibration plot (Fig. 4c). It was observed that the stability of the biosensor was maintained at up to 98.34% of its initial activity at 8 weeks. Following the completion of the eighth week, an increase in the biosensor response was seen. These results indicated that the developed PSA aptasensor had good stability for up to 8 weeks.

Detection of PSA in real human serum

One of the most crucial performance criteria for aptasensors is the capacity to analyze real samples. Since the serum PSA level is generally considered normal up to 4.0 ng/mL in healthy individuals [48], the samples were diluted with PB, considering this value to ensure the detection range before analysis in real serum samples. After diluting five different serum samples, the response of each serum sample on the aptasensor was determined, and these values were considered blank. Each serum sample was independently spiked with 250 and 500 fg/mL PSA. Serum PSA concentrations, and recovery values were computed using the equation of the calibration plot (Table 1).

The data in Table 1 show that our design yields highly accurate results in complex matrices. According to the real sample measurements, the PSA aptasensor offers remarkable clinical application potential, with excellent sensitivity. According to WHO standards, the variation in today's commercial serum PSA tests has decreased to 3–5%, and the detection thresholds have increased to 0.01–0.02 ng/mL for total PSA [62]. In this context, the system we have developed is also quite acceptable for the serum PSA detection limit determined by WHO.

Conclusion

In this study, we developed an electrochemical impedance spectroscopy-based aptasensor for highly sensitive and selective PSA analysis. The level of sensitivity we have achieved makes the proposed aptasensor one of the most sensitive biosensing systems in the literature. The LOD and LOQ values were determined as 8.74 and 29.13 fg/mL, respectively, while the dynamic range of the biosensor was 1.0–1500 fg/mL. The K_d value for the relevant aptamer was determined as 46.28±5.63 nM with the constructed novel biosensor. The aptasensor demonstrated high selectivity over IgG, haptoglobin, BSA, ascorbic acid, and glucose. The proposed aptasensor also provides adequate accuracy and satisfactory repeatability, reproducibility, and storage stability. Moreover, the aptasensor offered extremely sensitive and reliable results in detecting PSA levels in serum. In light of all these properties, it can be concluded that the developed aptasensor has enormous promise for PSA analysis in clinical applications.

Supplementary Information The online version contains supplementary material available at https://doi.org/10.1007/s00216-022-04309-8.

Funding This work was funded by the Çanakkale Onsekiz Mart University Council of Scientific Research Project [Project number: FBA-2020-3225].

Declarations

The serum samples used in this study were approved by the appropriate ethics committee (Namık Kemal University Ethics Committee) and the study was carried out in accordance with ethical standards.

Conflict of interest The authors declare no competing interests.

References

1. Ferlay J, Ervik M, Lam F, Colombet M, Mery L, Piñeros M, Bray F. Global cancer Observatory: cancer today. Lyon: international agency for research on cancer; 2018. https://gco.iarc.fr/today, Accessed 22 June 2022
2. Ashrafizadeh M, Paskeh MDA, Mirzaei S, Gholami MH, Zarrabi A, Hashemi F, Hushmandi K, Hashemi M, Nabavi N, Crea F, Ren J, Klionsky DJ, Kumar AP, Wang Y. Targeting autophagy in prostate cancer: preclinical and clinical evidence for therapeutic response. J Exp Clin Cancer Res. 2022;41:1–37. https://doi.org/10.1186/s13046-022-02293-6.
3. Merriel SWD, Pocock L, Gilbert E, Creavin S, Walter FM, Spencer A, Hamilton W. Systematic review and meta-analysis of the diagnostic accuracy of prostate-specific antigen (PSA) for the detection of prostate cancer in symptomatic patients. BMC Med. 2022;20:1–11. https://doi.org/10.1186/s12916-021-02230-y.
4. Stamey TA, Johnstone IM, McNeal JE, Lu AY, Yemoto CM. Preoperative serum prostate specific antigen levels between 2 and 22 ng./ml. correlate poorly with post-radical prostatectomy cancer morphology: Prostate specific antigen cure rates appear constant between 2 and 9 ng./ml. J Urol. 2002;167:103–11. https://doi.org/10.1016/S0022-5347(05)65392-X.
5. Barry MJ. Prostate-specific-antigen testing for early diagnosis of prostate cancer. Clin Pract. 2001;344:1373–7.
6. Westgard JO, Westgard SA. The quality of laboratory testing today: an assessment of σ metrics for analytic quality using performance data from proficiency testing surveys and the CLIA criteria for acceptable performance. Am J Clin Pathol. 2006;125(3):343–54.
7. CDC. Total Prostate-Specific Antigen (PSA) https://www.cdc.gov/nchs/data/nhanes/nhanes_03_04/l11psa_c_met_total_psa.pdf. Accessed 21 Aug 2022.
8. Ishibashi M. Standardization of prostate-specific antigen (PSA) assays: can interchangeability of PSA measurements be improved? Clin Chem. 2006;52(1):1–2.
9. Klein EA, Chait A, Hafron JM, Kernen KM, Manickam K, Stephenson AJ, Wagner M, Zhu H, Kestranek A, Zaslavsky B, Stovsky M. The Single-parameter, Structure-based IsoPSA Assay Demonstrates Improved Diagnostic Accuracy for Detection of Any Prostate Cancer and High-grade Prostate Cancer Compared to a Concentration-based Assay of Total Prostate-specific Antigen: A Preliminary Report. Eur Urol. 2017;72:942–9. https://doi.org/10.1016/j.eururo.2017.03.025.
10. Breault-Turcot J, Poirier-Richard HP, Couture M, Pelechacz D, Masson JF. Single chip SPR and fluorescent ELISA assay of prostate specific antigen. Lab Chip. 2015;15:4433–40. https://doi.org/10.1039/c5lc01045d.
11. Łupicka-Słowik A, Grzywa R, Leporowska E, Procyk D, Oleksyszyn J, Sieńczyk M. Development and evaluation of an immunoglobulin Y-based ELISA for measuring prostate specific antigen in human serum. Ann Lab Med. 2019;39:373–80. https://doi.org/10.3343/alm.2019.39.4.373.
12. Adachi T, Moriya K, Esaki K. Clinical evaluation of chemiluminescence immunoassay PSA (ACS-PSA) for detection of prostate cancer. Hinyokika kiyo Acta Urologica Japonica. 1998;44(7):469–76.
13. Cao JT, Zhao LZ, Zhang WS, Ma SH, Liu YM. Engineering WS 2–Au–HRP-assisted multiple signal amplification strategy for chemiluminescence immunoassay of prostate specific antigen. New J Chem. 2021;45(28):12494–9.
14. Vural T, Yaman YT, Ozturk S, Abaci S, Denkbas EB. Electrochemical immunoassay for detection of prostate specific antigen based on peptide nanotube-gold nanoparticle-polyaniline immobilized pencil graphite electrode. J Colloid Interface Sci. 2018;510:318–26.
15. Abu-Bakr El-Bayoumy AS, Hessien Keshta AT, Sallam KM, Ebeid NH, Elsheikh HM, Bayoumy BES. Extraction, purification of prostate-specific antigen (PSA), and establishment of radioimmunoassay system as a diagnostic tool for prostate disorders. J Immunoassay Immunochem. 2018;39(1):12–29.
16. You PY, Li FC, Liu MH, Chan YH. Colorimetric and fluorescent dual-mode immunoassay based on plasmon-enhanced fluorescence of polymer dots for detection of PSA in whole blood. ACS Appl Mater Interfaces. 2019;11(10):9841–9.
17. Crulhas BP, Karpik AE, Delella FK, Castro GR, Pedrosa VA. Electrochemical aptamer-based biosensor developed to monitor PSA and VEGF released by prostate cancer cells. Anal Bioanal Chem. 2017;409:6771–80. https://doi.org/10.1007/s00216-017-0630-1.
18. Pourmadadi M, Nouralishahi A, Shalbaf M, Shabani Shayeh J, Nouralishahi A. An electrochemical aptasensor for detection of prostate-specific antigen-based on carbon quantum dots-gold nanoparticles. Biotechnol Appl Biochem. 2022;1–9. https://doi.org/10.1002/bab.2340.
19. Zhao R, Zhao L, Feng H, Chen X, Zhang H, Bai Y, Feng F, Shuang S. A label-free fluorescent aptasensor based on HCR and G-quadruplex DNAzymes for the detection of prostate-specific

antigen. Analyst. 2021;146:1340–5. https://doi.org/10.1039/d0an02188a.
20. Ouhibi A, Raouafi A, Lorrain N, Guendouz M, Raouafi N, Moadhen A. Functionalized SERS substrate based on silicon nanowires for rapid detection of prostate specific antigen. Sens Actuators B. 2021;330:129352. https://doi.org/10.1016/j.snb.2020.129352.
21. Ding Y, Lu H, Shi G, Liu J, Shen G, Yu R. Cell-based immobilization strategy for sensitive piezoelectric immunoassay of total prostate specific antigen. Biosens Bioelectron. 2008;24:228–32. https://doi.org/10.1016/j.bios.2008.03.020.
22. Pohanka M. QCM biosensor for Prostate Specific Antigen assay using antibody – gold particle conjugate. Int J Electrochem Sci. 2021;16:1–9. https://doi.org/10.20964/2021.05.04.
23. Özyurt C, Uludağ İ, İnce B, Sezgintürk MK. Biosensing strategies for diagnosis of prostate specific antigen. J Pharm Biomed Anal. 2022;209. https://doi.org/10.1016/j.jpba.2021.114535.
24. Hassani S, Maghsoudi AS, Akmal MR, Rahmani S, Sarihi P, Ganjali MR, Norouzi P, Abdollahi M. A sensitive aptamer-based biosensor for electrochemical quantification of PSA as a specific diagnostic marker of prostate cancer. J Pharm Pharm Sci. 2020;23:243–58. https://doi.org/10.18433/jpps31171.
25. Li X, Shen L, Zhang D, Qi H, Gao Q, Ma F, Zhang C. Electrochemical impedance spectroscopy for study of aptamer-thrombin interfacial interactions. Biosens Bioelectron. 2008;23:1624–30. https://doi.org/10.1016/j.bios.2008.01.029.
26. Bahner N, Reich P, Frense D, Menger M, Schieke K, Beckmann D. An aptamer-based biosensor for detection of doxorubicin by electrochemical impedance spectroscopy. Anal Bioanal Chem. 2018;410:1453–62. https://doi.org/10.1007/s00216-017-0786-8.
27. Eissa S, Siaj M, Zourob M. Aptamer-based competitive electrochemical biosensor for brevetoxin-2. Biosens Bioelectron. 2015;69:148–54. https://doi.org/10.1016/j.bios.2015.01.055.
28. Armbruster DA, Pry T. Limit of blank, limit of detection and limit of quantitation. Clin Biochem Rev. 2008;29(Suppl 1):49.
29. Shrivastava A, Gupta V. Methods for the determination of limit of detection and limit of quantitation of the analytical methods. Chronicles Young Sci. 2011;2(1):21–25. https://doi.org/10.4103/2229-5186.79345.
30. Arshavsky-Graham S, Urmann K, Salama R, Massad-Ivanir N, Walter JG, Scheper T, Segal E. Aptamers vs. antibodies as capture probes in optical porous silicon biosensors. Analyst. 2020;145(14):4991–5003. https://doi.org/10.1039/d0an00178c.
31. Hulme EC, Trevethick MA. Ligand binding assays at equilibrium: validation and interpretation. Br J Pharmacol. 2010;161(6):1219–37. https://doi.org/10.1111/j.1476-5381.2009.00604.x.
32. Goutelle S, Maurin M, Rougier F, Barbaut X, Bourguignon L, Ducher M, Maire P. The Hill equation: a review of its capabilities in pharmacological modelling. Fundam Clin Pharmacol. 2008;22(6):633–48.
33. Thompson IM, Pauler DK, Goodman PJ, Tangen CM, Lucia MS, Parnes HL, Coltman Jr C.A. Prevalence of prostate cancer among men with a prostate-specific antigen level ≤ 4.0 ng per milliliter. N Engl J Med. 2004;350(22):2239–46.
34. Aydın EB, Sezgintürk MK. A sensitive and disposable electrochemical immunosensor for detection of SOX2, a biomarker of cancer. Talanta. 2017;72:162–70. https://doi.org/10.1016/j.talanta.2017.05.048.
35. Park K. Impedance Technique-Based Label-Free Electrochemical Aptasensor for Thrombin Using Single-Walled Carbon Nanotubes-Casted Screen-Printed Carbon Electrode. Sensors. 2022;22. https://doi.org/10.3390/s22072699.
36. İnce B, Sezgintürk MK. A high sensitive and cost-effective disposable biosensor for adiponectin determination in real human serum samples. Sens Actuators B. 2021;328. https://doi.org/10.1016/j.snb.2020.129051.
37. Lindholm-Sethson B, Nyström J, Malmsten M, Ringstad L, Nelson A, Geladi P. Electrochemical impedance spectroscopy in label-free biosensor applications: Multivariate data analysis for an objective interpretation. Anal Bioanal Chem. 2010;398:2341–9. https://doi.org/10.1007/s00216-010-4027-7.
38. Fan K, Zhu J, Wu X, Zhang X, Wang S, Wen W. A flexible label-free electrochemical aptasensor based on target-induced conjunction of two split aptamers and enzyme amplification. Sens Actuators B. 2022;363:131766. https://doi.org/10.1016/j.snb.2022.131766.
39. Zainol Abidin AS, Rahim RA, Huan CY, Mohd Maidin NN, Ahmad NA, Ba Hashwan SS, Mohd Faudzi FN, Hong VC. The Effect of Aptamer Concetration towards Reduced Graphene Oxide-Field Effect Transistor Surface Channel for Biosensor Application. IOP Conf Ser. Mater Sci Eng A. 2018;318. https://doi.org/10.1088/1757-899X/318/1/012045.
40. Akgün M, Kemal SM. A novel biosensing system based on ITO-single use electrode for highly sensitive analysis of VEGF. Int J Environ Anal Chem. 2020;100:432–50. https://doi.org/10.1080/03067319.2019.1709637.
41. González-Guerrero AB, Alvarez M, Castaño AG, Domínguez C, Lechuga LM. A comparative study of in-flow and micro-patterning biofunctionalization protocols for nanophotonic silicon-based biosensors. J Colloid Interface Sci. 2013;393:402–10. https://doi.org/10.1016/j.jcis.2012.10.040.
42. Avilés F, Sierra-Chi CA, Nistal A, May-Pat A, Rubio F, Rubio J. Influence of silane concentration on the silanization of multiwall carbon nanotubes. Carbon N Y. 2013;57:520–9. https://doi.org/10.1016/j.carbon.2013.02.031.
43. Özcan B, Demirbakan B, Yeşiller G, Sezgintürk MK. Introducing a new method for evaluation of the interaction between an antigen and an antibody: Single frequency impedance analysis for biosensing systems. Talanta. 2014;125:7–13. https://doi.org/10.1016/j.talanta.2014.02.067.
44. Zhen J, Liang G, Chen R, Jia W. Label-free hairpin-like aptamer and EIS-based practical, biostable sensor for acetamiprid detection. PLoS One. 2020;15:1–13. https://doi.org/10.1371/journal.pone.0244297.
45. Sarabaegi M, Roushani M, Hosseini H, Saedi Z, Lemraski EG. A novel ultrasensitive biosensor based on NiCo-MOF nanostructure and confined to flexible carbon nanofibers with high-surface skeleton to rapidly detect Helicobacter pylori. Mater Sci Semicond Process. 2022;139:106351. https://doi.org/10.1016/j.mssp.2021.106351.
46. Roychoudhury A, Dear JW, Bachmann TT. Proximity sensitive detection of microRNAs using electrochemical impedance spectroscopy biosensors. Biosens Bioelectron. 2022;212:114404. https://doi.org/10.1016/j.bios.2022.114404.
47. Najeeb MA, Ahmad Z, Shakoor RA, Mohamed AMA, Kahraman R. A novel classification of prostate specific antigen (PSA) biosensors based on transducing elements. Talanta. 2017;168:52–61. https://doi.org/10.1016/j.talanta.2017.03.022.
48. Savory N, Abe K, Sode K, Ikebukuro K. Selection of DNA aptamer against prostate specific antigen using a genetic algorithm and application to sensing. Biosens Bioelectron. 2010;26:1386–91. https://doi.org/10.1016/j.bios.2010.07.057.
49. Jolly P, Tamboli V, Harniman RL, Estrela P, Allender CJ, Bowen JL. Aptamer-MIP hybrid receptor for highly sensitive electrochemical detection of prostate specific antigen. Biosens Bioelectron. 2016;75:188–95. https://doi.org/10.1016/j.bios.2015.08.043.
50. Jolly P, Formisano N, Tkáč J, Kasák P, Frost CG, Estrela P. Label-free impedimetric aptasensor with antifouling surface chemistry: A prostate specific antigen case study. Sens Actuators B. 2015;209:306–12. https://doi.org/10.1016/j.snb.2014.11.083.
51. Meng W, Zhang W, Zhang J, Chen X, Zhang Y. An electrochemical immunosensor for prostate specific antigen using

nitrogen-doped graphene as a sensing platform. Anal Methods. 2019;11:2183–9. https://doi.org/10.1039/c9ay00064j.
52. Li Z, Yin J, Gao C, Qiu G, Meng A, Li Q. The construction of electrochemical aptasensor based on coral-like poly-aniline and Au nano-particles for the sensitive detection of prostate specific antigen. Sens Actuators B. 2019;295:93–100. https://doi.org/10.1016/j.snb.2019.05.070.
53. Wang Y, Feng D, Kan X. The combination of highly efficient resonance energy transfer in one nanocomposite and ferrocene-quenching for ultrasensitive electrochemiluminescence bioanalysis. Biosens Bioelectron. 2022;210:114347. https://doi.org/10.1016/j.bios.2022.114347.
54. Zhao J, Ma Z. Ultrasensitive detection of prostate specific antigen by electrochemical aptasensor using enzyme-free recycling amplification via target-induced catalytic hairpin assembly. Biosens Bioelectron. 2018;102:316–20. https://doi.org/10.1016/j.bios.2017.11.044.
55. Fernando PUAI, Glasscott MW, Kosgei GK, Cobb JS, Alberts EM, Bresnahan CG, Schutt TC, George GW, Moores LC. Toward Rational Design of Electrogenerated Molecularly Imprinted Polymers (eMIPs): Maximizing Monomer/Template Affinity. ACS Appl Polym Mater. 2021;3:4523–33. https://doi.org/10.1021/acsapm.1c00575.
56. Souada M, Piro B, Reisberg S, Anquetin G, Noël V, Pham MC. Label-free electrochemical detection of prostate-specific antigen based on nucleic acid aptamer. Biosens Bioelectron. 2015;68:49–54. https://doi.org/10.1016/j.bios.2014.12.033.
57. Liu S, Huo Y, Bai J, Ning B, Peng Y, Li S, Han D, Kang W, Gao Z. Rapid and sensitive detection of prostate-specific antigen via label-free frequency shift Raman of sensing graphene. Biosens Bioelectron. 2020;158:112184. https://doi.org/10.1016/j.bios.2020.112184.
58. Formisano N, Jolly P, Bhalla N, Cromhout M, Flanagan SP, Fogel R, Limson JL, Estrela P. Optimisation of an electrochemical impedance spectroscopy aptasensor by exploiting quartz crystal microbalance with dissipation signals. Sens Actuators B. 2015;220:369–75. https://doi.org/10.1016/j.snb.2015.05.049.
59. Díaz-Fernández A, Miranda-Castro R, de-los-Santos-Álvarez N, Lobo-Castañón MJ, Estrela P. Impedimetric aptamer-based glycan PSA score for discrimination of prostate cancer from other prostate diseases. Biosens Bioelectron. 2021;175. https://doi.org/10.1016/j.bios.2020.112872.
60. Malvano F, Albanese D, Pilloton R, Di Matteo M. A new label-free impedimetric aptasensor for gluten detection. Food Control. 2017;79:200–6. https://doi.org/10.1016/j.foodcont.2017.03.033.
61. Kong RM, Zhang X, Ding L, Yang D, Qu F. Label-free fluorescence turn-on aptasensor for prostate-specific antigen sensing based on aggregation-induced emission–silica nanospheres. Anal Bioanal Chem. 2017;409:5757–65. https://doi.org/10.1007/s00216-017-0519-z.
62. Scatena R. Advances in Cancer Biomarkers: From biochemistry to clinic for a critical revision. Springer. 2015;867.

Canan Özyurt has been Assistant Professor at Çanakkale Onsekiz Mart University, Çanakkale, Turkey, since 2019. She has been working for several years on developing genetically encoded biosensor approaches, aptamer selection, aptasensors, and electrochemical biosensing systems.

İnci Uludağ has been a research assistant at Çanakkale Onsekiz Mart University since 2019. She conducts scientific studies in the Biosensors and Lateral Flow Assay Laboratories. She works in particular on the development of biosensor systems for cancer biomarkers. Her research interests include life sciences, biochemistry, biotechnology, and electrochemistry.

Mustafa Kemal Sezgintürk is Professor in the Bioengineering Department at the Çanakkale Onsekiz Mart University, where he has been a faculty member since 2016. His research interests lie in the areas of biochemistry, biosensors, cancer biomarkers, electrochemical impedance spectroscopy, LFA-based biosensing systems, enzymology, protein purification, and characterization.